Glioma Pathogenesis-Related Protein 1 Exerts Tumor Suppressor Activities through Proapoptotic Reactive Oxygen Species–c-Jun–NH_2 Kinase Signaling

Likun Li,[1] ElMoataz Abdel Fattah,[1] Guangwen Cao,[1] Chengzhen Ren,[1] Guang Yang,[1] Alexei A. Goltsov,[1] A. Craig Chinault,[2] Wei-Wen Cai,[2] Terry L. Timme,[1] and Timothy C. Thompson[1,3,4]

[1]Scott Department of Urology, Departments of [2]Human and Molecular Genetics, [3]Molecular and Cellular Biology, and [4]Radiology, Baylor College of Medicine, Houston, Texas

Abstract

***Glioma pathogenesis-related protein 1* (*GLIPR1*), a novel p53 target gene, is down-regulated by methylation in prostate cancer and has p53-dependent and -independent proapoptotic activities in tumor cells. These properties suggest an important tumor suppressor role for *GLIPR1*, yet direct genetic evidence of a tumor suppressor function for *GLIPR1* is lacking and the molecular mechanism(s), through which *GLIPR1* exerts its tumor suppressor functions, has not been shown. Here, we report that the expression of GLIPR1 is significantly reduced in human prostate tumor tissues compared with adjacent normal prostate tissues and in multiple human cancer cell lines. Overexpression of GLIPR1 in cancer cells leads to suppression of colony growth and induction of apoptosis. Mice with an inactivated *Glipr1* gene had significantly shorter tumor-free survival times than either *Glipr1*$^{+/+}$ or *Glipr1*$^{+/-}$ mice in both *p53*$^{+/+}$ and *p53*$^{+/-}$ genetic backgrounds, owing to their development of a unique array of malignant tumors. Mechanistic analysis indicated that GLIPR1 up-regulation increases the production of reactive oxygen species (ROS) leading to apoptosis through activation of the c-Jun–NH_2 kinase (JNK) signaling cascade. Thus, our results identify *GLIPR1* as a proapoptotic tumor suppressor acting through the ROS-JNK pathway and support the therapeutic potential for this protein.** [Cancer Res 2008;68(2):434–43]

Introduction

Glioma pathogenesis-related protein 1 (*GLIPR1*) was originally identified in human glioblastoma (1) with subsequent designation of related to testes-specific, vespid, and pathogenesis protein 1 (*RTVP1*; ref. 2; HGNC approved gene symbol, *GLIPR1*). Its activity was thought to be associated with myelomonocytic differentiation toward the macrophage phenotype (3); however, using differential display PCR to screen for p53 target genes in prostate cancer, we identified *Glipr1* (mouse counterpart of *GLIPR1*; HGNC approved gene symbol, *Glipr1*) in mice as one of the p53 target genes (4) and later confirmed that both *Glipr1* and *GLIPR1* contain p53 response elements and are up-regulated by both p53 and DNA damage–inducing agents (4, 5). We also observed that GLIPR1 expression in human prostate cancer, especially in metastatic tumors, is significantly reduced compared with that in normal prostate, owing to methylation in the regulatory region of this gene in prostate cancer cells (5). Functional analysis revealed that overexpression of either Glipr1 or GLIPR1 induces apoptosis and suppresses colony formation *in vitro* in various mouse and human cancer cell lines, independently of p53 status (4, 5). Adenoviral vector–mediated delivery of *Glipr1* into orthotopic mouse prostate cancer significantly suppressed tumor growth and metastasis to lung (6), whereas administration of a novel *Glipr1* gene modified tumor cell vaccine to mice had significant antitumor activity in a preclinical model of recurrent prostate cancer (7). Adenoviral vector–mediated *GLIPR1* gene therapy is currently in a phase I/phase II clinical trial (IND13033), and GLIPR1 protein therapy is in preclinical development. The progress in our GLIPR1 studies and its promising potential in clinical applications prompted us to pursue direct genetic evidence for *GLIPR1* as a tumor suppressor and to identify the molecular mechanism(s) through which *GLIPR1* exerts its tumor suppressor functions.

The candidacy of *GLIPR1* as a tumor suppressor and a novel proapoptotic gene raises the critical issue of the downstream pathways responsible for GLIPR1-associated cell death. Many lines of evidence suggest that reactive oxygen species (ROS) function as a pivotal component in a proapoptotic signaling cascade (8–10). ROS free radicals are required for metabolism in normal cells but can also cause direct cellular damage or can function as intermediate signaling molecules, leading to oxidative stress and a series of biological consequences, including the induction of apoptosis (reviewed in refs. 8, 11, 12).

The induction of ROS-mediated apoptosis depends on signaling by apoptosis signal-regulated kinase 1 (ASK1), mitogen-activated protein/extracellular signal-regulated kinase kinase (MEK), and c-Jun–NH_2 kinase (JNK; refs. 9, 11, 13). Although the involvement of JNK in apoptosis remains controversial, emerging evidence favors the concept that sustained JNK activation leads to apoptosis in a wide spectrum of cells, although the mechanisms of this effect are not fully understood (14–16).

Here, we present direct genetic evidence supporting an independent tumor suppressor role for *GLIPR1* and show that its activities are not limited to prostate cancer but extend to multiple human malignancies. GLIPR1-mediated apoptosis in cancer cells seems to require signaling through the ROS-ASK1-MEK4/7-JNK pathway.

Note: Supplementary data for this article are available at Cancer Research Online (http://cancerres.aacrjournals.org/).

Requests for reprints: Timothy C. Thompson, The University of Texas M. D. Anderson Cancer Center, Unit 1374, Department of Genitourinary Medical Oncology, 1515 Holcombe Boulevard, Houston, TX 77030. Phone: 713-792-9955; Fax: 713-792-9956; E-mail: timthomp@mdanderson.org.

doi:10.1158/0008-5472.CAN-07-2931

Materials and Methods

Tissues, cell lines, and reagents. Normal or tumor human prostate tissues were obtained with informed consent and maintained by the Baylor College of Medicine Specialized Program of Research Excellence in prostate cancer tissue bank. Other human tissue RNAs were purchased from BD Biosciences Clontech. HCT116*p53*$^{+/+}$ and HCT116*p53*$^{-/-}$ were gifts from Dr. B. Vogelstein of Johns Hopkins University. Other cancer cell lines were purchased from American Type Culture Collection. CM-H_2DCFDA was from Invitrogen/Molecular Probes. Doxycycline, butylated hydroxyanisole (BHA), and monoclonal antibody to β-actin were from Sigma. SP600125 was from CalBiochem. JNK1 and JNK2 small interfering RNA (siRNA; siRNA ID 1320 and 1547, respectively), and siPORTAmine were from Ambion. Polyclonal GLIPR1 and Glipr1 antibodies were generated as described previously (4). Apoptosis-inducing factor (AIF) polyclonal and cytochrome *c* monoclonal antibodies were from BD PharMingen. c-Jun polyclonal antibody was from Santa Cruz. The remainder of the antibodies were from Cell Signaling.

Analysis of GLIPR1 expression. Total RNA from human tissues or cancer cell lines was extracted with the RiboPure RNA extraction kit (Ambion). Reverse transcription (RT) reactions were carried out with the high-capacity cDNA archive kit (Applied Biosystem) according to the manufacturer's protocol. PCR reactions were performed as previously described (5, 17) using the following Taqman probes and primers (Applied Biosystems): Hs00199268_m1 for GLIPR1 and Hs99999905_m1 for glyceraldehyde-3-phosphate dehydrogenase (GAPDH). Real-time PCR was performed with the ABI PRISM 7000 sequence detection system (Applied Biosystems) according to the manufacturer's instructions. The relative quantity of GLIPR1 mRNA was determined by the $\Delta\Delta C_T$ method as described by the manufacturer and normalized to GAPDH RNA in the same cDNA preparation.

Apoptotic analysis and clonogenic assay. Apoptotic nuclear morphology was analyzed with fluorescence microscopy and a computer-assisted counting program (Nucleotech) after 4′,6-diamidino-2-phenylindole (DAPI) staining (2 μg/mL). DNA fragmentation analysis was performed using cell death ELISA (Roche). For clonogenic assays, 10 to 14 days after reseeding of GLIPR1-expressing or control cells (1×10^4 cells per 10-cm plate for LNCaP and 1×10^3 cells per 10-cm plate for the remainder of cell lines), colonies were stained with 3-(4,5-dimethylthiazol-2-yl)-2,5-diphenyltetrazolium bromide and counted by use of a phase contrast microscope and a computer-assisted colony counting program.

Generation of mice. *Glipr1*$^{-/-}$ mice were generated from embryonic stem cells transduced with the targeting vector (Supplementary Fig. S1). Targeted embryonic stem cell clones were used to create chimeric mice by injection of embryonic stem cells into blastocysts from C57BL/6JTyr$^{c\text{-}Brd}$ mice. A chimeric male was mated with C57BL/6JTyr$^{c\text{-}Brd}$ females, and germline transmission of the mutant allele was verified by Southern blot analysis and PCR of genomic DNA from the tails of agouti coat-colored offspring. Primers were promoter region sense F1, 5′-GAA GTC CGG TGT AAG TTT CGT G-3′, exon 1 antisense R1, 5′-GCT GCG GGG TTC TGA TAG A-3′, and targeting vector antisense R2, 5′-CCC TTC CCA GCC TCT GAG-3′. Mice from *Glipr1*$^{+/-}$ intercrosses were genotyped by Southern blotting and PCR and evaluated at 2 months of age unless otherwise noted. All mice used in the experiments were C57BL6/129Sv hybrid (1:1) and were maintained in facilities accredited by the American Association for Accreditation of Laboratory Animal Care. All experiments were conducted in accordance with the principles and procedures outlined in NIH's Guide for the Care and Use of Laboratory Animals. *p53*$^{-/-}$ mice were maintained as previously described (18). *Glipr1*$^{-/-}$ mice were bred with *p53*$^{-/-}$ mice to obtain *p53*$^{+/-}$;*Glipr1*$^{+/-}$ offspring. Mice with different genetic status of *p53* and *Glipr1* (*p53*$^{+/+}$;*Glipr1*$^{+/+}$, *p53*$^{+/+}$;*Glipr1*$^{+/-}$, *p53*$^{+/+}$;*Glipr1*$^{-/-}$, *p53*$^{+/-}$;*Glipr1*$^{+/+}$, *p53*$^{+/-}$;*Glipr1*$^{+/-}$, *p53*$^{+/-}$;*Glipr1*$^{-/-}$, *p53*$^{-/-}$;*Glipr1*$^{+/+}$, *p53*$^{-/-}$;*Glipr1*$^{+/-}$ and *p53*$^{-/-}$;*Glipr1*$^{-/-}$) were generated by breeding *p53*$^{+/-}$;*Glipr1*$^{+/-}$ mice. Genotypes of mice were determined by PCR using specific primer sets for *Glipr1* and *p53*.

Survival analysis. *Glipr1* genetic studies were performed using mice with *p53*$^{+/+}$ or *p53*$^{+/-}$ genetic background. Six groups of mice, *p53*$^{+/+}$;*Glipr1*$^{+/+}$ (n = 58), *p53*$^{+/+}$;*Glipr1*$^{+/-}$ (n = 77), *p53*$^{+/+}$;*Glipr1*$^{-/-}$ (n = 38), *p53*$^{+/-}$;*Glipr1*$^{+/+}$ (n = 63), *p53*$^{+/-}$;*Glipr1*$^{+/-}$ (n = 104), and *p53*$^{+/-}$;*Glipr1*$^{-/-}$(n = 74), were maintained according to standard animal maintenance protocol. Histopathologic analysis was used to determine that death was associated with the presence of specific malignancies. The number of surviving mice was determined on a daily basis, and all deaths due to unknown causes were excluded from the analysis. Survival times were converted to Kaplan-Meier plots, with the log-rank test used for statistical comparisons.

Histopathologic evaluation. All tissues were fixed in 10% neutral formalin, processed for paraffin embedding and made into 5-μm sections. The sections were stained with H&E following a routine procedure and were evaluated under a Zeiss Axioplan microscope.

Genotype confirmation. A subset of tumor tissues from each genotype group (n = 5) and mouse embryo fibroblast (MEF) isolates derived from *p53*$^{+/+}$;*Glipr1*$^{+/+}$ (n = 3) and *p53*$^{+/+}$;*Glipr1*$^{-/-}$(n = 3) mice were subjected to full-length DNA sequencing to verify the fidelity of *p53* and *Glipr1* genetic status. Total RNA was isolated and purified from the tumor tissues, and *p53* and *Glipr1* cDNAs were prepared by RT-PCR using specific sets of primers: *p53*, sense 5′-CCTTCCCAGCAGGGTGTCA-3′ and antisense 5′-GACGG-GATGCAGAGGCAGT-3′; *Glipr1*, sense 5′-GGTCCAGCAGCAACCAGAGA-3′ and antisense 5′-GCCGCATGTGATTCAGTTGT-3′. DNA sequencing was performed using ABI Prism 310 automatic DNA sequencer. Mutation or deletion was checked against published *p53* and *Glipr1* DNA sequences in the database.

Loss of heterozygosity analysis. Loss of wild-type *p53* allele in tumors derived from cohorts of *p53*$^{+/-}$ mice was determined by Southern hybridization as described previously (5). Briefly, a 600-bp KpnI fragment of the mouse *p53* cDNA spanning exons 2 to 6 was prepared from plasmid LR10, randomly labeled with α-^{32}P-dCTP and hybridized to *Bam*HI-digested normal or tumor genomic DNA after electrophoresis and transfer to a nylon membrane. Radioactive-labeled DNA was visualized by exposing the hybridized membrane to Kodak film at −80°C. The same samples were analyzed by PCR as described in genotyping. Radiographic images were analyzed by densitometry for the signal ratios of wild-type p53 bands (migrating at 5.0 kb) to the mutant allele bands (migrating at 6.5kb). A ratio of 60% to 100% was considered no loss of heterozygosity (LOH), a ratio of 30% to 60% was considered partial LOH, and a ratio of 0% to 30% was considered LOH.

ROS detection and measurement. ROS were measured as described previously (19, 20). Briefly, after incubation of cells with 5 μmol/L CM-H_2DCFDA in a phenol red–free and serum-free medium for 1 h, the medium was removed and the cells were washed twice with ice-cold PBS and lysed in a luciferase buffer (19). ROS levels in the cell lysates were measured using a GENios fluorescence reader with 485-nm excitation wavelength and 535-nm emission wavelength. For ROS detection by fluorescence microscopy, cells were incubated with 5 μmol/L CM-H_2DCFDA as described above, washed twice, and replaced with regular medium, and the fluorescence of the oxidized product, CM-DCF, was visualized with a fluorescence microscope.

Inhibitor studies. R24 cells were incubated with 1 μg/mL of doxycycline for 24 and 48 h in the presence or absence of specified concentrations of BHA, SP600125, or Z-VAD-FMK. Western analyses were performed 24 h posttreatment, whereas apoptosis was analyzed 24 h later. In siRNA experiments, R24 cells were transfected with indicated concentrations of JNK1 and JNK2 siRNA, using siPORTAmine 24 h before GLIPR1 induction by doxycycline. Gene suppression was examined by quantitative RT-PCR (qRT-PCR), with DAPI staining used to analyze apoptosis 48 h after doxycycline induction.

MEF culture and treatment of MEF with doxorubicin and etoposide. Primary MEF were obtained from day 14.5 embryos and propagated according to standard 3T3 protocol. Briefly, each embryo was decapitated, thoroughly minced, and trypsinized in 5mL of trypsin-EDTA for 30 min at 37°C. MEF isolates were grown in complete DMEM. Early passage primary MEF (≤5) were used for the experiments. Subconfluent *Glipr1*$^{+/+}$ and *Glipr1*$^{-/-}$ MEF were treated with 5 μmol/L doxorubicin or 50 μmol/L etoposide for 24 or 48 h, as indicated in the specific experiments, followed by qRT-PCR analysis, ROS measurement, Western blotting, or apoptosis analysis.

Statistical analysis. The log-rank test was used for the statistical analysis of mouse tumor-free survival. Fisher's exact test was used for statistical comparisons of LOH frequencies between different cohorts of mice. Paired *t* test was used for statistical comparisons of GLIPR1 expression in normal or malignant human prostate tissues, and unpaired *t* test was used in other experiments in which probability levels were determined. A *P* value of <0.05 was considered statistically significant.

Results

GLIPR1 is reduced in multiple types of human cancer cells, and its up-regulation suppresses colony formation and induces apoptosis. We previously reported that GLIPR1 expression is decreased in prostate cancer cells compared with normal cells and in human prostate cancer tissues compared with adjacent normal prostate tissues (4, 5). Using an expanded number of human prostate cancer samples (n = 31), we confirmed this observation in human prostate cancer tissues compared with adjacent normal prostate tissues (P = 0.0076; Fig. 1*A*). To generalize the down-regulation of GLIPR1 in cancer, we analyzed GLIPR1 mRNA expression using quantitative PCR in different types of human tissues and in sarcoma, lymphoma, prostate cancer, bladder cancer, lung cancer, and colon cancer cell lines. The results showed high levels of GLIPR1 mRNA both in nontransformed cells and normal tissues (Fig. 1*B, open columns*) but strikingly reduced levels in all cancer cell lines examined (*solid columns*). These data suggest selective down-regulation of GLIPR1 in cancer cells.

Because suppressed GLIPR1 expression is common in human cancer, we asked whether enforced expression of this gene could lead to apoptosis in affected cells. After adenoviral vector–mediated transduction of human prostate epithelial cells and four human cancer cell lines (LNCaP prostate, TSU-Pr1 bladder, H1299 lung, and KHOS-312H sarcoma), clonogenic assays showed that expression of GLIPR1 leads to significant reductions in colony formation in cancer cells (Fig. 1*C*; $P < 0.05$ or $P < 0.0001$). Analysis by DAPI staining (Fig. 1*D, left*) and DNA fragmentation ELISA (Fig. 1*D, right*) showed minimal apoptotic effect on prostate epithelial cells but showed substantially increased apoptosis in the same set of cancer cell lines ($P < 0.05$ or $P < 0.0001$). These results, obtained with adenoviral vector–mediated gene delivery, were validated in doxycycline-mediated gene induction experiments

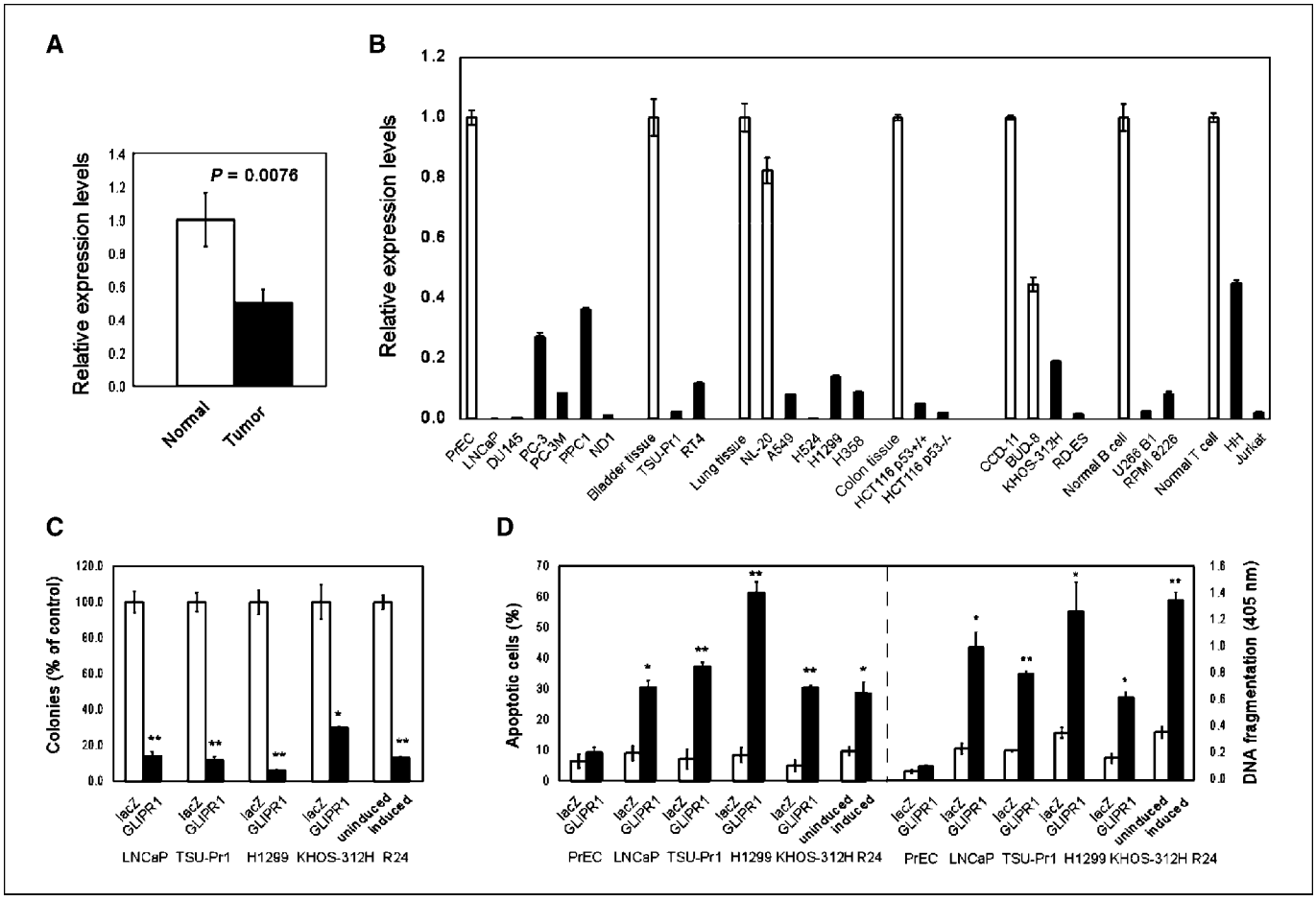

Figure 1. GLIPR1 expression in normal and malignant prostate tissues and in different cancer cell lines, and the consequences of its up-regulation in cancer cells. *A,* RT-PCR analysis of GLIPR1 mRNA levels in 31 prostate tumor samples and adjacent normal prostate tissue samples. Statistical analysis was performed with a paired *t* test. *B,* RT-PCR analysis of GLIPR1 mRNA levels in different types of cancer cells and their normal cell or tissue counterpart. Cell strains/lines used were obtained from the American Type Culture Collection or as indicated include the following: PrEC, normal prostatic epithelial cells; LNCaP, DU145, PC-3, PC-3M, PPC1 and ND1, prostate cancer cells; TSU-Pr1 and RT4, bladder cancer cells; NL-20, normal lung epithelial cells; A549, H524, H1299 and H358, lung cancer cells; HCT116p53$^{+/+}$ and HCT116p53$^{-/-}$, colon cancer cells; CCD-11, normal lung fibroblast cell line; BUD-8, normal skin fibroblasts cell line; KH0S-312H and RD-ES, sarcoma cells; U266B1 and RPMI8226, B-cell lymphoma; HH, T-cell lymphoma cell line; Jurkat, T-cell leukemia cell line. *Solid columns,* cancer cell lines; *open columns,* their normal cell or tissue counterparts. *C,* clonogenic assays of AdGLIPR1 or AdLacz-infected cancer cells and doxycycline-induced or uninduced R24 cells. *D,* apoptotic analysis of AdGLIPR1 or AdLacZ-infected cancer cells and doxycycline-induced or uninduced R24 cells by DAPI staining and DNA fragmentation ELISA. *, $P < 0.05$; **, $P < 0.0001$ by unpaired *t* test.

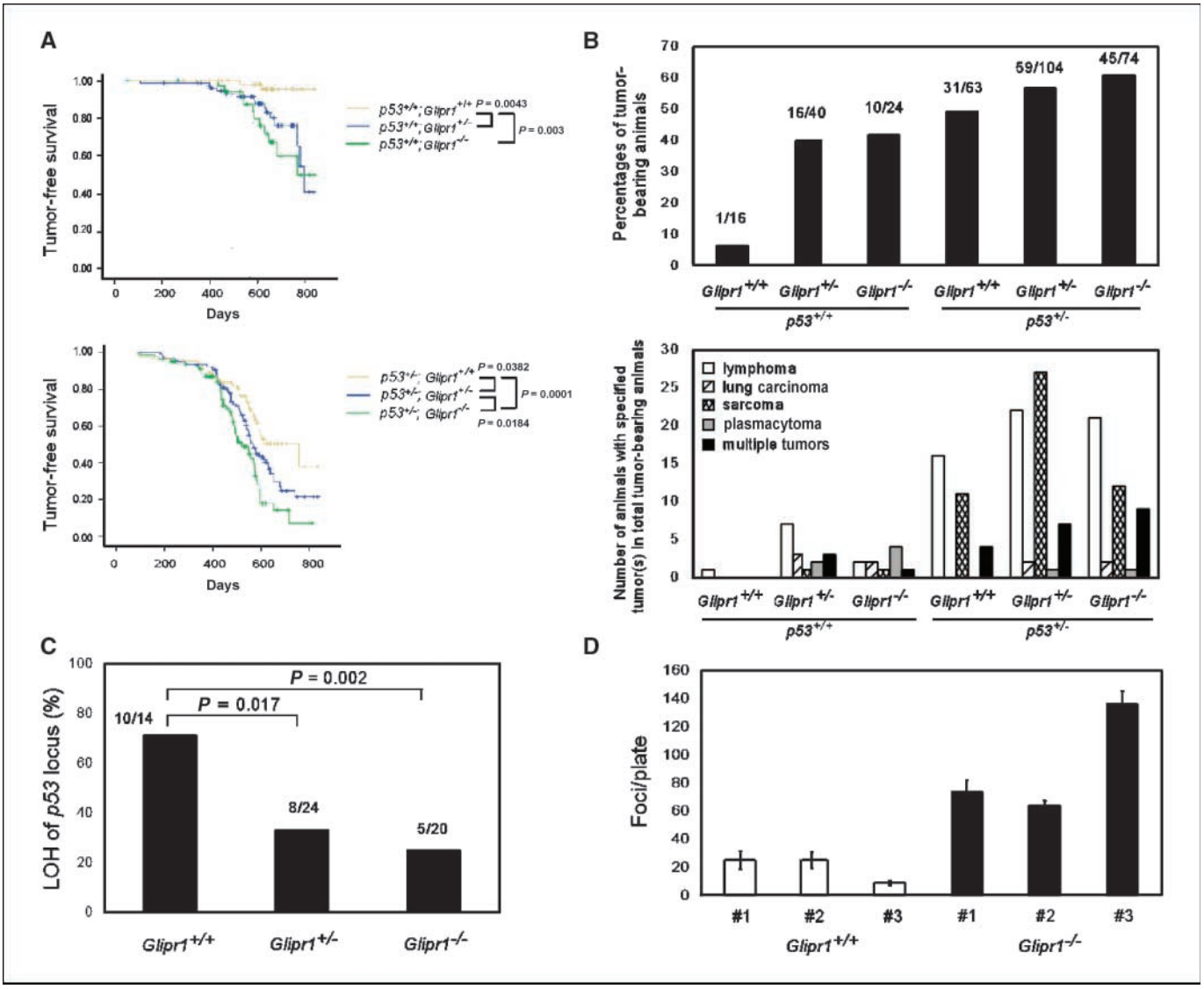

Figure 2. Loss of *Glipr1* predisposes mice to tumorigenesis and increases transformation potential in MEFs. *A,* tumor-free survival of $Glipr1^{+/+}$, $Glipr1^{+/-}$, and $Glipr1^{-/-}$ mice was monitored daily for >2 y. Survival times were converted to Kaplan-Meier plots and compared by the log-rank test for statistical differences. *Top,* $p53^{+/+}$ cohorts: $p53^{+/+}$;$Glipr1^{+/+}$ ($n = 32$), $p53^{+/+}$;$Glipr1^{+/-}$ ($n = 68$), and $p53^{+/+}$;$Glipr1^{-/-}$ ($n = 27$); *bottom,* $p53^{+/-}$ cohorts: $p53^{+/-}$;$Glipr1^{+/+}$ ($n = 63$), $p53^{+/-}$;$Glipr1^{+/-}$ ($n = 104$), and $p53^{+/-}$;$Glipr1^{-/-}$ mice ($n = 74$). *B,* frequencies and spectrum of tumors in $Glipr1^{+/+}$, $Glipr1^{+/-}$, and $Glipr1^{-/-}$ mice with wild-type or heterozygous *p53* genetic background. *Top,* percentages of tumor-bearing animals. The fractions above the columns indicate the number of animals analyzed that had tumors. *Bottom,* spectrum of tumors. *C,* loss of wild-type *p53* allele in tumors derived from cohorts of $p53^{+/-}$ mice was determined by Southern hybridization (Supplementary Fig. S3). The ratio of the wild-type *p53* band (migrating at 5.0 kb) to the mutant allele band (migrating at 6.5 kb) was analyzed by densitometry. A ratio of 60% to 100% was considered no LOH, a ratio of 30% to 60% percent was considered partial LOH, and a ratio of 0% to 30% was considered LOH. The fractions above the bars indicate the number of tumors analyzed that had LOH. Statistical comparisons of $Glipr1^{+/-}$ or $Glipr1^{-/-}$ tumors to $Glipr1^{+/+}$ tumors were performed using Fisher's exact test. *D,* $p53^{+/+}$;$Glipr1^{+/+}$ and $p53^{+/+}$;$Glipr1^{-/-}$ MEFs were infected with Zipras/myc9 (21). Cells were reseeded at a density of 1×10^6 cells per 10-cm plate, and focus assays were performed 10-14 d later. $P = 0.033$ by unpaired *t* test.

using a TSU-Pr1 GLIPR1 tet-on stable clone, R24, in which induction of GLIPR1 expression resulted in remarkable reduction in colony formation (Fig. 1*C, far right*; $P < 0.0001$) and significant increase in apoptosis (Fig. 1*D, left and right, far right*; $P < 0.05$ and $P < 0.0001$, respectively). We hypothesize from these *in vitro* experiments that *GLIPR1* is a proapoptotic gene and likely tumor suppressor in multiple types of cancer cells.

Loss of *Glipr1* predisposes mice to tumorigenesis and increases transformation potential in mouse embryonic fibroblasts. To test the predicted tumor suppressor role of *Glipr1 in vivo*, we analyzed the rates of survival and spontaneous malignancies in $Glipr1^{+/+}$, $Glipr1^{+/-}$, and $Glipr1^{-/-}$ mice with a $p53^{+/+}$ or $p53^{+/-}$ genetic background. As shown in Fig. 2*A, top*, both the $p53^{+/+}$;$Glipr1^{+/-}$ and $p53^{+/+}$;$Glipr1^{-/-}$ groups had significantly decreased tumor-free survival rates compared with that for the $p53^{+/+}$;$Glipr1^{+/+}$ group ($P = 0.004$ and 0.003, respectively), suggesting that loss of *Glipr1* predisposes mice to tumorigenesis in the presence of wild-type p53. As expected, in the cohorts of mice with $p53^{+/-}$ genetic background, the $p53^{+/-}$;$Glipr1^{+/-}$ and $p53^{+/-}$;$Glipr1^{-/-}$ groups also showed significantly reduced tumor-free survival rates compared with that for the $p53^{+/-}$;$Glipr1^{+/+}$ group ($P = 0.038$ and 0.0001, respectively; Fig. 2*A, bottom*). Frequencies and spectrum of tumors in these six genotypes of mice are detailed in Fig. 2*B*, and representative histologic samples were shown in

Supplementary Fig. S2. The data show that loss of *Glipr1* leads to a wild spectrum of malignancies in mice. Analysis of the prostates from these mice did not reveal any malignancies. No mutation or deletion was found from the randomly picked subsets of tumors of all six genotypes after full-length cDNA sequencing of p53 and *Glipr1*.

Because mice with heterozygous p53 are susceptible to loss of the remaining wild-type p53 allele under oncogenic stimulation (18), we analyzed LOH of the p53 locus in cohorts of $p53^{+/-}$;$Glipr1^{+/+}$, $p53^{+/-}$;$Glipr1^{+/-}$, and $p53^{+/-}$;$Glipr1^{-/-}$ mice. Interestingly, within the three cohorts of $p53^{+/-}$ mice, the frequency of LOH of the p53 locus was highest in $p53^{+/-}$;$Glipr1^{+/+}$ tumor (71%) and lowest in $p53^{+/-}$;$Glipr1^{-/-}$ tumor (25%; Fig. 2*C* and Supplementary Fig. S3), suggesting that loss of *Glipr1* plays a critical and independent role in tumorigenecity. Thus, our genetic data strongly support a novel tumor suppressor function with broad organ specificity for *Glipr1*.

To further asses the importance of *Glipr1* in malignant transformation, we transformed $p53^{+/+}$;$Glipr1^{+/+}$ and $p53^{+/+}$;$Glipr1^{-/-}$ MEF with an oncogenic *v-Ha-ras* + *v-gag-myc* retroviral vector (21), as *Myc* has been shown to contribute to oxidative stress resistance through a glutathione-directed survival pathway, and this activity may play a role in *Ras* + *Myc* oncogenic transformation (22). Using the well-established focus formation assay, we found that loss of *Glipr1* function potentiates the transformation capacity of *v-Ha-ras* + *v-gag-myc* expression, with an average of >4-fold foci in $Glipr1^{-/-}$ MEF compared with $Glipr1^{+/+}$ MEF (Fig. 2*D*). Together with the results of our tumor-free survival analysis, these data strongly indicate a critical role for *Glipr1* in preventing spontaneous tumor development and oncogene-mediated transformation.

GLIPR1 overexpression results in elevated ROS levels and activation of the ASK1-MEK4/7-JNK signaling cascade. What are the mechanisms of apoptosis induced by GLIPR1 in cancer cells? GLIPR1 protein shows sequence homology with members of the cysteine-rich secretory protein (CRISP) family, which harbor a distinct cysteine-rich domain at the carboxy terminus (17). Cysteine residues can be modified to various products that are thought to be the predominant means of redox modifications within mammalian cells (23, 24). We therefore hypothesized that GLIPR1 overexpression may affect cellular ROS generation. To test this hypothesis, we monitored ROS levels using a fluorescent probe, CM-H_2DCFDA, which is nonfluorescent until it is oxidized by ROS within the cell. The representative fluorescent microscopic images in Fig. 3*A* show ROS levels in doxycycline-uninduced (*left*) and doxycycline-induced (*right*) parental cells TSU-Pr1 (*top*) and R24 cells (*bottom*). Notably, doxycycline does not induce ROS in TSU-Pr1 cells, demonstrating the specificity of doxycycline-mediated GLIPR1 induction in R24 cells. Quantitative spectrofluorometric measurements of ROS levels in lysates prepared from LNCaP, PC-3, H1299, KO947 (a mouse sarcoma cell line), and R24 cancer cells showed that GLIPR1 overexpression causes significantly higher ROS production compared with controls (Fig. 3*B*; $P < 0.05$). These data support our working hypothesis that GLIPR1 up-regulation leads to an increase in ROS production, which may represent a critical step in GLIPR1-mediated apoptosis in cancer cells.

Several lines of evidence indicate that JNK signaling is a major element of ROS-mediated apoptosis (9, 11, 13), leading us to ask if this pathway is involved in GLIPR1-mediated ROS production and apoptosis. To address this question, we determined the protein levels and phosphorylation state of key components of the JNK signaling cascade, using R24 cells with either induced or uninduced expression of GLIPR1. Western blotting analysis showed that overexpression of GLIPR1 activates a series of kinases in the JNK signaling cascade. At 16 h postinduction, ASK1, MEK4/7, and JNK were phosphorylated and remained in that activated state over the next 32 h of the study, whereas c-Jun showed delayed phosphorylation (Fig. 3*C*). There was no obvious change in the level of any of these proteins. Importantly, the sustained activation of JNK is typically associated with apoptosis induction (9, 25).

Because Akt, mitogen-activated protein kinases p42/44, and p38 are often involved in decisions of cell survival or death (26–28), we also asked whether these molecules/pathways contribute to GLIPR1-mediated apoptosis. As shown in Fig. 3*D*, the protein levels and the phosphorylation state of Akt, p42/44, or p38 were relatively unchanged after induction of GLIPR1 expression. Together, these findings suggest that activation of the ASK1-MEK4/7-JNK pathway is a specific consequence of GLIPR1 up-regulation.

Requirement for increased ROS generation and activation of the JNK pathway in GLIPR1-mediated apoptosis. To assess the contribution of ROS in GLIPR1-mediated apoptosis, we treated R24 cells with doxycycline in the presence or absence of the antioxidant BHA. Subsequent analysis of ROS levels, the JNK signaling pathway and apoptosis showed that the treatment of cells with BHA resulted in significant reduction of cellular ROS levels (Fig. 4*A, top*), significant suppression of MEK4/7 and JNK phosphorylation (Fig. 4*B*), and remarkable reduction of GLIPR1-mediated apoptosis (Fig. 4*A, bottom*). These data indicate that increased ROS generation is indeed required for GLIPR1-mediated activation of JNK and ultimately the induction of apoptosis.

To establish the role of JNK activation in GLIPR1-mediated apoptosis, we used a JNK-specific chemical inhibitor, SP600125, to inhibit JNK activities before the induction of GLIPR1. As expected, SP600125 effectively inhibits the phosphorylation of JNK and its downstream target c-Jun (Fig. 4*C, top*), the cleavage of PARP and GLIPR1-mediated apoptosis (Fig. 4*C, bottom*) in a dose-dependent manner. The role of JNK in GLIPR1-mediated apoptosis was also shown by transfecting R24 cells with JNK1 and JNK2 siRNAs before GLIPR1 induction with doxycycline (Fig. 4*D*).

Down-regulation of Bcl-2 and activation of caspases are associated with GLIPR1-mediated apoptosis. To determine the downstream molecular events after JNK activation, we examined Bcl-2 family proteins, caspases, and other mitochondrial death pathway–related molecules. The levels of proapoptotic Bcl-2 family members Bax, Bid, Bad, and Bim, as well as the phosphorylation of Bad and Bim, were relatively unchanged after GLIPR1 induction (Supplementary Fig. S4); however, the level of Bcl-2 protein was slightly reduced at 24 h and further reduced at 48 h (Fig. 5*A*). Phosphorylation of Bcl-2 at Ser^{70} and at Thr^{56} was increased after doxycycline induction (Fig. 5*A*). The activities of certain caspases (8, 9, 7, and 3) were significantly enhanced, as indicated by their cleavage, as well as by the cleavage of PARP (Fig. 5*B*). Analysis of specific apoptosis-related proteins in isolated mitochondrial and cytosolic fractions showed a lower Bcl-2 level in mitochondria but not in the cytosol of doxycycline-induced R24 cells (Fig. 5*C*). Given the reduced expression and increased phosphorylation of Bcl-2 in GLIPR1-stimulated cells (Fig. 5*A*), we considered that induction of GLIPR1 expression in R24 cells might lead to increased Bcl-2 translocation from mitochondrial to cytosolic sites. Moreover, overexpression of GLIPR1 caused the release of AIF and cytochrome *c* from mitochondria into cytosol (Fig. 5*C*). Thus, because the balance between proapoptotic and antiapoptotic Bcl-2 family proteins in mitochondria is a critical factor in apoptosis induction whereas the release of AIF and cytochrome *c* can activate

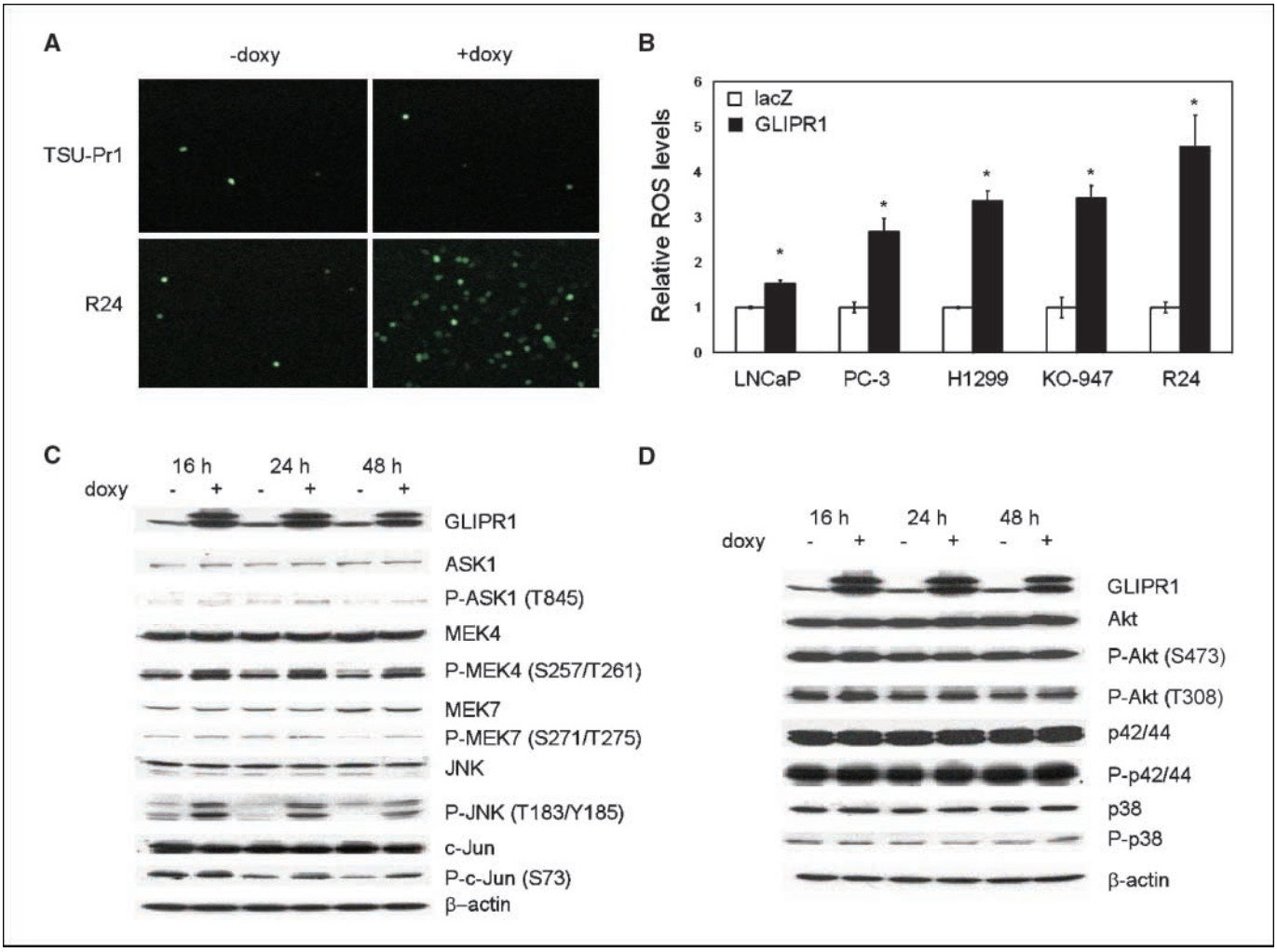

Figure 3. GLIPR1 overexpression results in elevated ROS levels and the activation of the ASK1-MEK4/7-JNK signaling cascade. *A,* representative images showing ROS-positive cells in doxycycline-induced and uninduced TSU-Pr1 and R24 cells after incubation of cells with 5 μmol/L CM-H_2DCFDA for 1 h. *B,* after adenoviral vector–mediated gene transduction and incubation of cells with 5 μmol/L CM-H_2DCFDA for 1 h, ROS levels in the cell lysates were measured with a GENios fluorescence reader with 485-nm excitation wavelength and 535-nm emission wavelength. The data are reported as fold increases over controls. *, $P < 0.05$, by unpaired *t* test. *C,* activation of the ASK1-MEK4/7-JNK signaling cascade by GLIPR1 expression in R24 cells. Cells were grown in media with or without 1 μg/mL of doxycycline (*doxy*) for the indicated times. Activation of the ASK1-MEK4/7-JNK signaling cascade is indicated by phosphorylation of specific residues of kinases known to be required for kinase activities. β-actin was used as the loading control. *D,* the expression and phosphorylation of Akt, p42/44, and p38 in doxycycline-induced or uninduced R24 cells.

the Apaf1-caspase 9 complex, DNA fragmentation, and chromatin condensation (29–31), it seemed reasonable to suggest that mitochondrial dysfunction caused by GLIPR1 overexpression contributes to GLIPR1-mediated apoptosis. To test whether GLIPR1-mediated apoptosis is caspase-dependent, we pretreated R24 cells with Z-VAD-FMK, a broad-range caspase inhibitor, for 1 h before the induction of GLIPR1 expression with doxycycline. The data presented in Fig. 5*D* shows that caspase inhibitor effectively but not completely inhibited GLIPR1-mediated apoptosis. We conclude that GLIPR1 may induce apoptosis through both caspase-dependent and caspase-independent mechanisms.

Mechanisms of Glipr1-mediated apoptosis in *p53*$^{+/+}$;*Glipr1*$^{+/+}$ and *p53*$^{+/+}$;*Glipr1*$^{-/-}$ MEF. To substantiate the apparent mechanisms of GLIPR1-medated apoptosis in cancer cells, we used *p53*$^{+/+}$;*Glipr1*$^{+/+}$ and *p53*$^{+/+}$;*Glipr1*$^{-/-}$ MEF to test whether *Glipr1* affects cellular ROS generation, JNK signaling, and apoptosis in response to the DNA damage–inducing agents doxorubicin and etoposide, both of which can up-regulate *Glipr1* expression (4). Using DNA sequencing, we confirmed that none of the MEF isolates contain mutation or deletion in *p53* and none of the *Glipr1*$^{+/+}$ MEF isolates contain mutation or deletion in *Glipr1*, and using quantitative RT-PCR, we confirmed that all MEF isolates express *p53* and only *Glipr1*$^{+/+}$ MEF isolates express *Glipr1* (Supplementary Fig. S5). We also found that exposure of *Glipr1*$^{+/+}$ MEF cells to doxorubicin and etoposide resulted in higher expression of Glipr1 mRNA compared with that in DMSO-treated cells (Fig. 6*A*; $P < 0.05$). Western blotting analysis also showed increased Glipr1 protein expression (Fig. 6*C*). Moreover, although treatment with doxorubicin and etoposide substantially increased ROS generation above basal levels in both *Glipr1*$^{+/+}$ and *Glipr1*$^{-/-}$ MEF isolates (data not shown), ROS levels in *Glipr1*$^{+/+}$ MEF isolates were significantly higher than those in *Glipr1*$^{-/-}$ MEF isolates (Fig. 6*B*; $P < 0.05$). JNK activities in doxorubicin-treated or etoposide-treated *Glipr1*$^{+/+}$ and *Glipr1*$^{-/-}$ MEF isolates were then evaluated by Western blotting analysis (Fig. 6*C, left and middle*) together with quantitative densitometry analysis (Fig. 6*C, right*). JNK activities in

DMSO (control)–treated *Glipr1*$^{+/+}$ and *Glipr1*$^{-/-}$ MEF did not show significant differences; however, *Glipr1*$^{+/+}$ MEF showed significantly higher JNK activities than *Glipr1*$^{-/-}$ MEF after treatment with doxorubicin or etoposide (Fig. 6*C*). Consistent with the increased ROS generation and JNK activities, *Glipr1*$^{+/+}$ MEF treated with doxorubicin or etoposide showed significantly increased apoptotic activities compared with results for *Glipr1*$^{-/-}$ MEF (Fig. 6*D*; $P < 0.05$). Thus, the proapoptotic signaling mechanisms attributed to GLIPR1 in cancer cells seem to be similar in DNA-damaged embryonic fibroblasts.

Discussion

In this study, we show selective GLIPR1 down-regulation in multiple tumor types, whereas enforced expression of GLIPR1 caused suppression of colony growth and massive apoptosis. These findings build on our previous observations that *Glipr1/GLIPR1* is a direct target gene of p53 with proapoptotic activities and that its expression is suppressed in prostate cancer (4, 5). More importantly, because the lack of p53-mediated apoptosis plays a key role in tumorigenesis and progression (32–36), down-regulation of GLIPR1 in different cancers supports a tumor suppressor role for this proapoptotic gene. In contrast, a recent report shows that GLIPR1 (RTVP-1) is overexpressed in gliomas and promotes the growth, survival, and invasion of glioma cells (37). Thus, the functions of GLIPR1 in glial tumors seem to occur within a unique biological context that cannot be directly compared with prostate cancer and other tumor types examined in the present study, in which GLIPR1 is highly expressed in normal cells/tissues but is down-regulated in tumors.

A tumor suppressor function for GLIPR1 is also supported by previous studies of the effects of GLIPR1 overexpression both *in vitro* and *in vivo* (4–7, 17); however, direct genetic evidence of such function was lacking until this study. We now show that

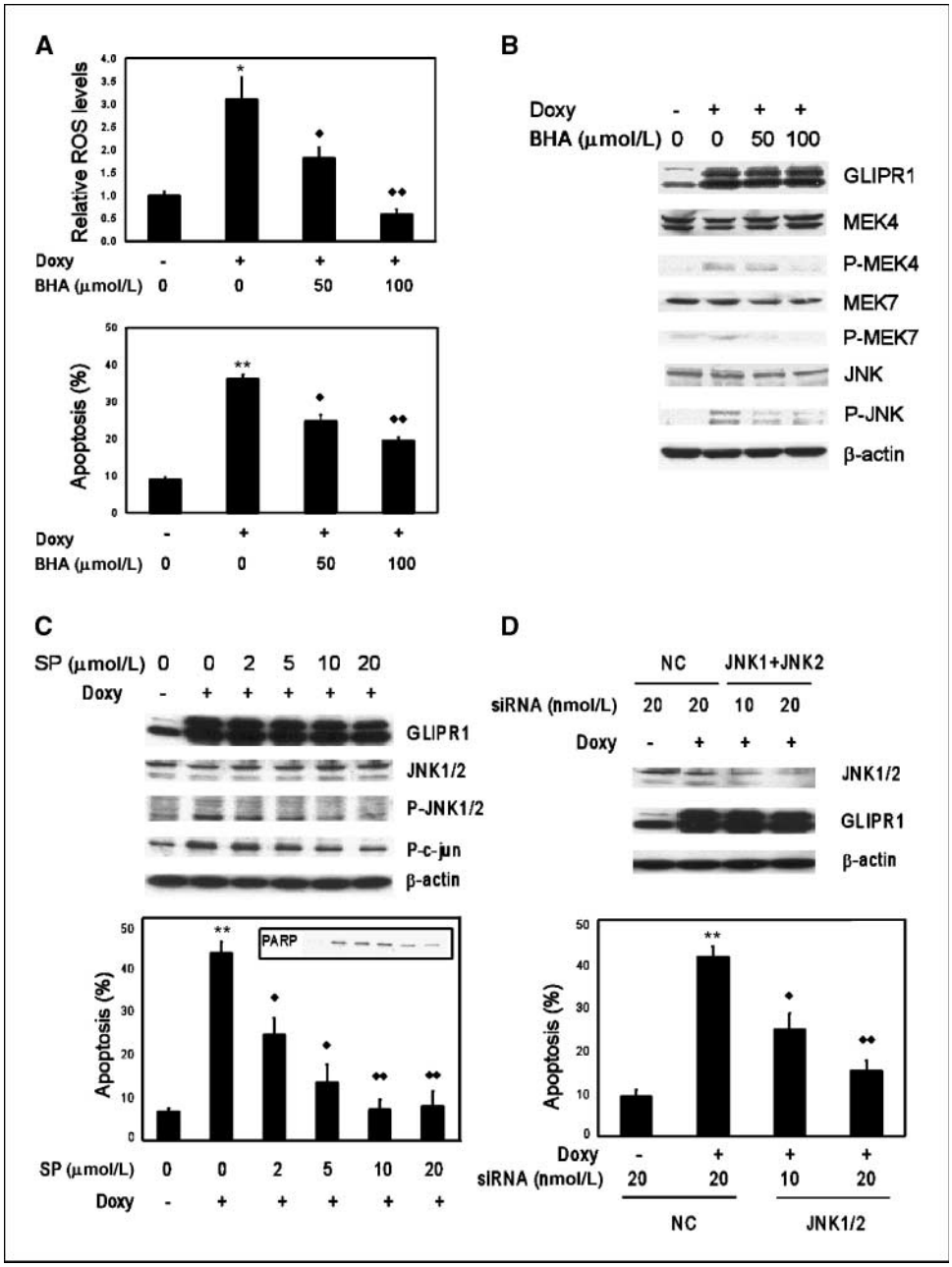

Figure 4. ROS generation and JNK activation are required for GLIPR1-mediated apoptosis. *A,* antioxidant BHA effectively blocked production/accumulation of cellular ROS (*top*) and apoptosis (DAPI staining analysis, *bottom*). *B,* BHA abrogated the activation of MEK4/7 and JNK induced by GLIPR1 overexpression, as indicated by the reduction of phosphorylation of MEK4/7 and JNK at specific residues. β-actin was used as the loading control. *C,* JNK-specific inhibitor SP600125 inhibits GLIPR1-mediated JNK and c-Jun activation (*top*) and apoptosis (DAPI staining analysis, *bottom*) in a dose-dependent manner. β-actin was used as the loading control. The insert in the bottom is a representative blot showing PARP cleavage. *D,* JNK1 + JNK2 siRNA effectively blocked JNK1/2 expression (*top*) and GLIPR1-mediated apoptosis (DAPI staining analysis, *bottom*). β-actin was used as the loading control. **, $P < 0.0001$ (compared with −doxycycline); ♦, $P < 0.05$ and ♦♦, $P < 0.0001$ (compared with +doxycycline) by unpaired *t* test.

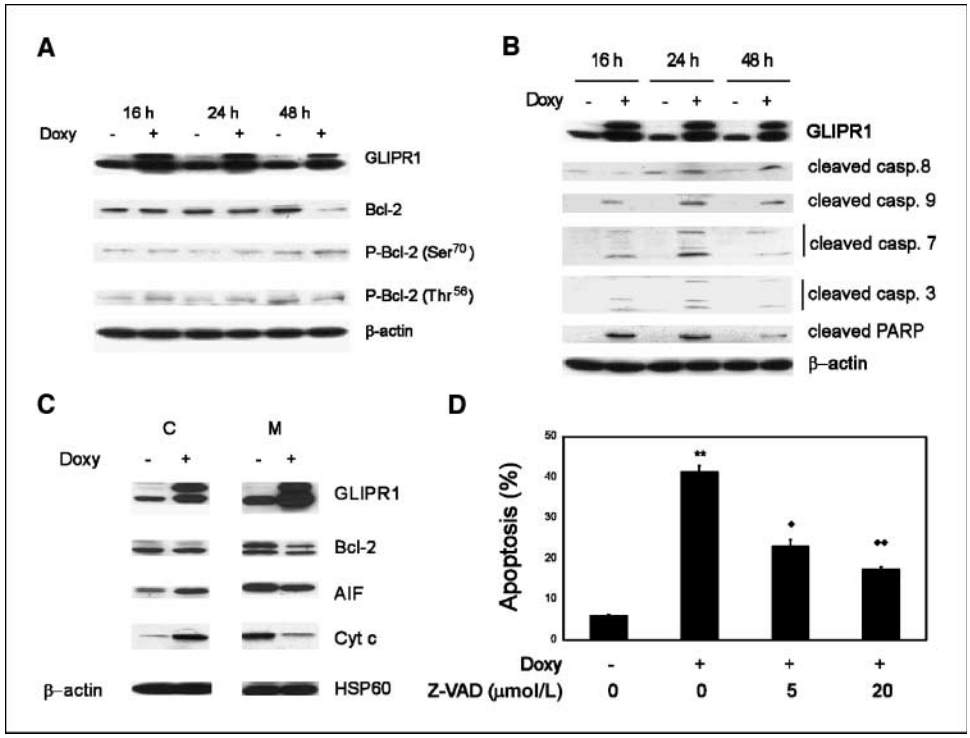

Figure 5. GLIPR1 overexpression causes inactivation of Bcl-2, dysfunction of mitochondria, and activation of a wide spectrum of caspases. *A,* GLIPR1 expression led to the reduction of Bcl-2 expression and the increase of phosphorylation of Bcl-2 at Ser^{70} and Thr^{56}. β-actin was used as the loading control. *B,* overexpression of GLIPR1 led to the activation of caspases 8, 9, 7, and 3 and to the cleavage of PARP, as indicated by the increased amount of cleaved forms of caspases and PARP. β-actin was used as the loading control. *C,* Western analysis of specific apoptosis-related proteins in cytosolic fraction (*C*) and mitochondrial fraction (*M*). β-actin and HSP60 were used as the loading control for the cytosolic and mitochondrial fractions, respectively. *D,* Z-VAD, a broad-range caspase inhibitor, significantly reduced GLIPR1-induced apoptosis. **, $P < 0.0001$ (compared with −doxycycline); ♦, $P < 0.05$; ♦♦, $P < 0.0001$ (compared with +doxycycline) by unpaired *t* test.

complete loss of *Glipr1* makes mice more vulnerable to spontaneous tumorigenesis, leading to the formation of a wide spectrum of tumors and significantly shorter tumor-free survival times in both $p53^{+/+}$ and $p53^{+/-}$ genetic background. Importantly, progressive loss of *Glipr1* in $p53^{+/-}$ background resulted in a low frequency of *p53* LOH (Fig. 2*C* and Supplementary Fig. S3). These data indicate that *Glipr1* has independent tumor suppressor functions under these conditions. The observed increase in tumor frequency and reduced survival in $Glipr1^{-/-}$ mice is noteworthy since mice with inactivating mutations in other proapoptotic p53 target genes, such as *Puma* and *Noxa*, failed to show increased numbers of tumors in limited studies (38). Moreover, we showed cooperativity between the loss of *Glipr1* function and *v-Ha-ras* + *v-gag-myc* overexpression in *Glipr1* MEF experiments. Because Myc-induced transformation may be related to the capacity of this oncogene to contribute to oxidative stress resistance (22), it is conceivable that this cooperative interaction plays a role in tumorigenesis *in vivo*.

The p53 family can regulate any of the well-characterized apoptotic pathways and likely others that have not been fully established. Our data indicate that GLIPR1 functions not in the classic p53-mediated intrinsic (mitochondrial) pathway but in a less well-defined signaling cascade, in which the increased production of ROS leads to apoptosis. Indeed, as a member of the CRISP family of proteins, GLIPR1 contains 11 cysteines that are concentrated in the carboxy terminus of the molecule (17). Because cysteine residues within polypeptides play an important role in redox homeostasis in mammalian cells (23, 24), this structural feature suggests a mechanistic link between GLIPR1 expression and the generation of ROS, although additional studies are needed to elucidate the biochemical and molecular underpinnings of this linkage. Given that ROS can function as a downstream mediator in p53-induced apoptosis (39) and that GLIPR1 is a direct target of p53 (4, 5) capable of inducing ROS generation by itself (Fig. 3*A* and *B*), we suggest that this novel tumor suppressor may function as an important mediator in the p53-induced increase of ROS.

Sustained activation of the ASK1-MEK4/7-JNK cascade plays a central role in ROS-mediated cell death (9, 13) and was a prominent finding in cells overexpressing GLIPR1 in our study. It is worthy noting that the involvement of JNK in apoptosis remains somewhat controversial. Its function in apoptosis or survival is context dependent. In our present study, we showed that activated JNK signaling is required for GLIPR1-mediated apoptosis in cancer cells. However, in a previous report (40), suppression of endogenous JNK caused inhibition of cell proliferation in normal prostate epithelial cells and five prostate cancer cell lines (LNCaP, DU145, CWR22v1, LAPC4, and PC-3) and induction of apoptosis in LNCaP and DU145 but not in CWR22v1, LAPC4, or PC-3. These results suggest that the apoptotic responses to JNK inhibition are cell line dependent. Extending this general observation, we offer the following argument as an explanation for the apparent differences between our results and these results. Under normal culture conditions, endogenous JNK expression does not cause cell death or the inhibition of cell proliferation. In fact, certain levels of JNK seem to be needed for normal cellular activities. In the cited study, the authors suppressed endogenous JNK activities by using a JNK inhibitor. However, in our study GLIPR1 overexpression significantly increased JNK activities beyond endogenous levels to a level that achieved the threshold for activation of a specific set of downstream proapoptotic targets. Actually, many lines of evidence from independent research groups have shown that JNK activation plays a critical role in apoptosis induced by various therapeutic agents in prostate cancer cells (13, 41–43). In summary, the function of JNK in apoptosis and survival remains controversial and is context dependent, yet sustained JNK activation by genetic manipulation or by therapeutic stimulation usually leads to apoptosis. Future

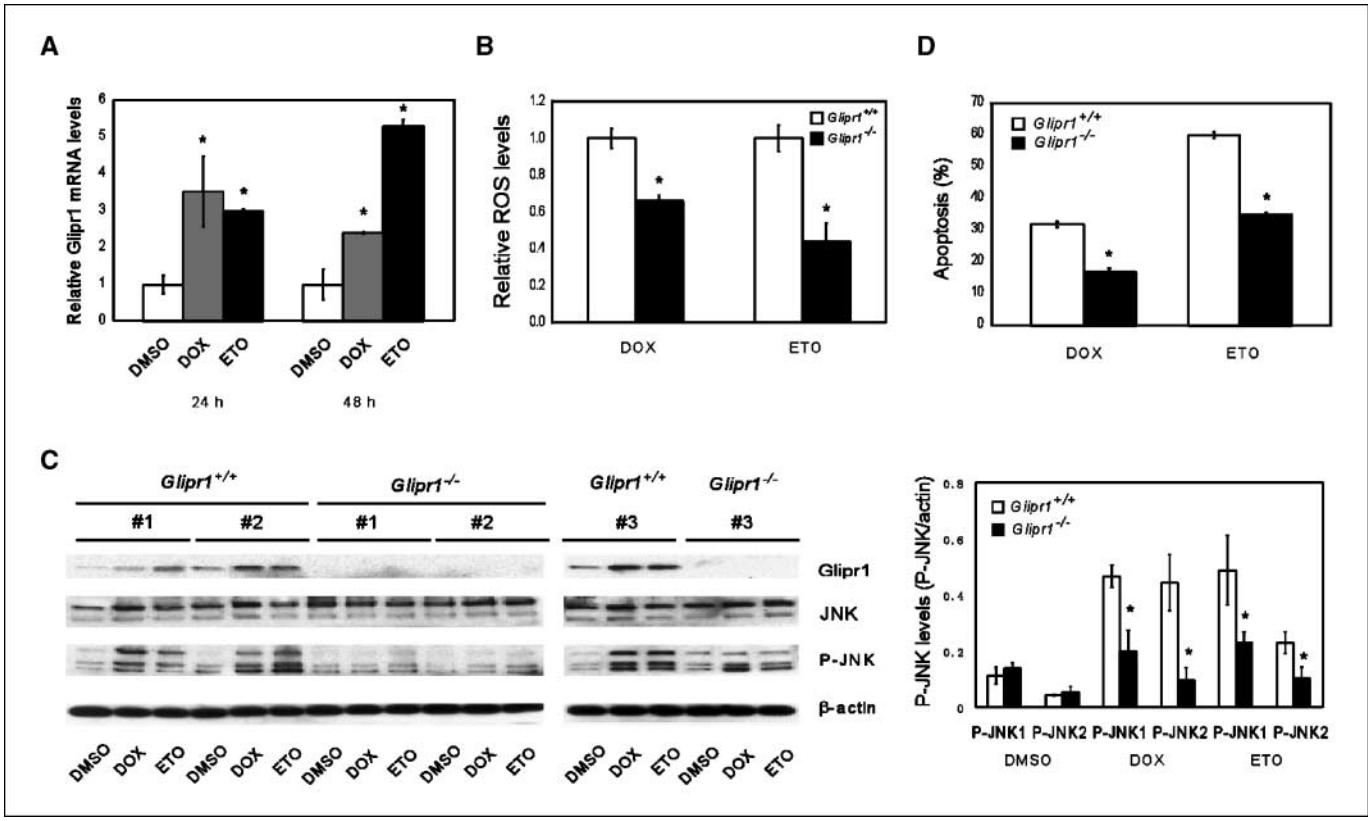

Figure 6. Loss of *Glipr1* reduces ROS levels, JNK activities, and apoptosis of MEF in response to the DNA-damaging agents that stimulate Glipr1 expression. *A, $p53^{+/+}$;$Glipr1^{+/+}$* MEF were treated with 5 μmol/L doxorubicin (*DOX*) or 50 μmol/L etoposide (*ETO*) for the indicated times, and Glipr1 mRNA levels were determined by qRT-PCR. *Columns,* means of three *$p53^{+/+}$;$Glipr1^{+/+}$* MEF isolates in two independent experiments; *bars,* SD. *, $P < 0.05$ by unpaired *t* test. *B, $p53^{+/+}$;$Glipr1^{+/+}$* and *$p53^{+/+}$;$Glipr1^{-/-}$* MEF were treated with 5 μmol/L doxorubicin or 50 μmol/L etoposide for 48 h before incubation with 5 μmol/L CM-H_2DCFDA for 1 h. ROS levels in the cell lysates were measured with a GENios fluorescence reader with 485-nm excitation wavelength and 535-nm emission wavelength. *Columns,* means of two *$p53^{+/+}$;$Glipr1^{+/+}$* MEF and two *$p53^{+/+}$;$Glipr1^{-/-}$* MEF in two independent experiments; *bars,* SD. *, $P < 0.05$ by unpaired *t* test. *C,* Western blotting analysis for JNK phosphorylation in DMSO (control)–treated, doxorubicin-treated, or etoposide-treated *$p53^{+/+}$;$Glipr1^{+/+}$* and *$p53^{+/+}$;$Glipr1^{-/-}$* MEF. β-actin was used as the loading control (*left and middle*). *Right,* densitometry analysis of P-JNK levels. The density readings for P-JNK1 and P-JNK2 were standardized to those of β-actin. *Columns,* means of three *$p53^{+/+}$;$Glipr1^{+/+}$* MEF and three *$p53^{+/+}$;$Glipr1^{-/-}$* MEF; *bars,* SD. *, $P < 0.05$ by unpaired *t* test. *D,* apoptotic analysis with DAPI staining for doxorubicin-treated or etoposide-treated *$p53^{+/+}$;$Glipr1^{+/+}$* and *$p53^{+/+}$;$Glipr1^{-/-}$* MEF. *Columns,* means of two *$p53^{+/+}$;$Glipr1^{+/+}$* MEF and two *$p53^{+/+}$;$Glipr1^{-/-}$* MEF in three independent experiments; *bars,* SD. *, $P < 0.05$ by unpaired *t* test.

studies are warranted to fully understand the mechanistic basis for the cell and context-dependent activities of JNK activation.

Interestingly, GLIPR1-induced ROS generation and JNK activation correlated within Bcl-2 phosphorylation at Ser^{70} and Thr^{56}, suggesting that Bcl-2 may function downstream of JNK. Multiple phosphorylation sites, including Thr^{56} and Ser^{70}, have been identified on Bcl-2 and are targets of ASK1-MEK7-JNK signaling (44, 45). Interestingly, phosphorylation of Bcl-2 at Thr^{56} and Ser^{70} favors p53-induced apoptosis (46). Finally, there was evidence of significant activation of caspases 8, 9, 7, and 3 in cells overexpressing GLIPR1. Interpreted together, these *in vitro* data suggest that GLIPR1-mediated apoptosis in cancer cells proceeds through induction of ROS generation, activation of the ASK1-MEK4/7-JNK signaling cascade, inactivation of Bcl-2 by both down-regulation of expression and phosphorylation, and activation of wide-spectrum caspases. The relevancy of these downstream events for mammalian systems was shown by comparison of the effects of DNA damaging drugs in MEF isolates from *$p53^{+/+}$;$Glipr^{+/+}$* and *$p53^{+/+}$;$Glipr^{-/-}$* mice.

The identification of *GLIPR1* as a novel, broad-spectrum tumor suppressor whose proapoptotic activities are exerted through ROS-ASK1-MEK4/7-JNK signaling has intriguing implications for the targeted therapy of human cancers. An increase of ROS has been shown to increase the susceptibility of tumor cells to chemotherapy, an effect that might augment the apoptotic consequences of ROS accumulation in a tumor cell–specific fashion (47–49). Thus, restoration of GLIPR1 function in cancer cells, using either gene or protein delivery methods, may provide a safe and effective strategy of targeted therapy for a range of human tumors. We have begun to test this concept through an ongoing neoadjuvant phase I/phase II clinical trial in which adenoviral vector–mediated GLIPR1 therapy is given by direct intratumoral injection (IND13033).

Acknowledgments

Received 8/3/2007; revised 9/27/2007; accepted 11/9/2007.

Grant support: National Cancer Institute grant R01-50588 and Baylor College of Medicine Specialized Program of Research Excellence in Prostate Cancer grant P50-58204.

The costs of publication of this article were defrayed in part by the payment of page charges. This article must therefore be hereby marked *advertisement* in accordance with 18 U.S.C. Section 1734 solely to indicate this fact.

We thank Dr. Allan Bradley for consultation regarding the generation of *Glipr1* knockout mice, Anna Frolov for assistance in statistical analysis, and Kellie Jane Poudrier for editorial assistance.

References

1. Murphy EV, Zhang Y, Zhu W, Biggs J. The human glioma pathogenesis-related protein is structurally related to plant pathogenesis-related proteins and its gene is expressed specifically in brain tumors. Gene 1995;159:131–5.

2. Rich T, Chen P, Furman F, Huynh N, Israel MA. RTVP-1, a novel human gene with sequence similarity to genes of diverse species, is expressed in tumor cell lines of glial but not neuronal origin. Gene 1996;180:125–30.

3. Gingras MC, Margolin JF. Differential expression of multiple unexpected genes during U937 cell and macrophage differentiation detected by suppressive subtractive hybridization. Exp Hematol 2000;28:350.

4. Ren C, Li L, Goltsov AA, et al. mRTVP-1, a novel p53 target gene with proapoptotic activities. Mol Cell Biol 2002;22:3345–57.

5. Ren C, Li L, Yang G, et al. RTVP-1, a tumor suppressor inactivated by methylation in prostate cancer. Cancer Res 2004;64:969–76.

6. Satoh T, Timme TL, Saika T, et al. Adenoviral vector-mediated mRTVP-1 gene therapy for prostate cancer. Hum Gene Ther 2003;14:91–101.

7. Naruishi K, Timme TL, Kusaka N, et al. Adenoviral vector-mediated RTVP-1 gene-modified tumor cell-based vaccine suppresses the development of experimental prostate cancer. Cancer Gene Ther 2006;17:17.

8. Engel RH, Evens AM. Oxidative stress and apoptosis: a new treatment paradigm in cancer. Front Biosci 2006;11:300–12.

9. Kamata H, Honda S, Maeda S, et al. Reactive oxygen species promote TNFα-induced death and sustained JNK activation by inhibiting MAP kinase phosphatases. Cell 2005;120:649–61.

10. Singh SV, Srivastava SK, Choi S, et al. Sulforaphane-induced cell death in human prostate cancer cells is initiated by reactive oxygen species. J Biol Chem 2005;280:19911–24.

11. Nakano H, Nakajima A, Sakon-Komazawa S, et al. Reactive oxygen species mediate crosstalk between NF-κB and JNK. Cell Death Differ 2006;13:730–7.

12. Zhang Y, Chen F. Reactive oxygen species (ROS), troublemakers between nuclear factor-κB (NF-κB) and c-Jun NH([2])-terminal kinase (JNK). Cancer Res 2004;64:1902–5.

13. Antosiewicz J, Herman-Antosiewicz A, Marynowski SW, Singh SV. c-Jun NH(2)-terminal kinase signaling axis regulates diallyl trisulfide-induced generation of reactive oxygen species and cell cycle arrest in human prostate cancer cells. Cancer Res 2006;66:5379–86.

14. Davis RJ. Signal transduction by the JNK group of MAP kinases. Cell 2000;103:239–52.

15. Deng Y, Ren X, Yang L, Lin Y, Wu X. A JNK-dependent pathway is required for TNFα-induced apoptosis. Cell 2003;115:61–70.

16. Liu J, Lin A. Role of JNK activation in apoptosis: a double-edged sword. Cell Res 2005;15:36–42.

17. Ren C, Ren CH, Li L, Goltsov AA, Thompson TC. Identification and characterization of RTVP1/GLIPR1-like genes, a novel p53 target gene cluster. Genomics 2006;88:163–72.

18. Thompson TC, Park SH, Timme TL, et al. Loss of p53 function leads to metastasis in ras+myc-initiated mouse prostate cancer. Oncogene 1995;10:869–79.

19. Chandel NS, Schumacker PT, Arch RH. Reactive oxygen species are downstream products of TRAF-mediated signal transduction. J Biol Chem 2001;276:42728–36.

20. Pham CG, Bubici C, Zazzeroni F, et al. Ferritin heavy chain up-regulation by NF-κB inhibits TNFα-induced apoptosis by suppressing reactive oxygen species. Cell 2004;119:529–42.

21. Thompson TC, Southgate J, Kitchener G, Land H. Multistage carcinogenesis induced by ras and myc oncogenes in a reconstituted organ. Cell 1989;56:917–30.

22. Benassi B, Fanciulli M, Fiorentino F, et al. c-Myc phosphorylation is required for cellular response to oxidative stress. Mol Cell 2006;21:509–19.

23. Fratelli M, Goodwin LO, Orom UA, et al. Gene expression profiling reveals a signaling role of glutathione in redox regulation. Proc Natl Acad Sci U S A 2005;102:13998–4003.

24. Shelton MD, Chock PB, Mieyal JJ. Glutaredoxin: role in reversible protein s-glutathionylation and regulation of redox signal transduction and protein translocation. Antioxid Redox Signal 2005;7:348–66.

25. Wullaert A, Heyninck K, Beyaert R. Mechanisms of crosstalk between TNF-induced NF-κB and JNK activation in hepatocytes. Biochem Pharmacol 2006;72:1090–101.

26. Li L, Ittmann MM, Ayala G, et al. The emerging role of the PI3-K-Akt pathway in prostate cancer progression. Prostate Cancer Prostatic Dis 2005;8:108–18.

27. Pearson G, Robinson F, Beers Gibson T, et al. Mitogen-activated protein (MAP) kinase pathways: regulation and physiological functions. Endocr Rev 2001;22:153–83.

28. Wada T, Penninger JM. Mitogen-activated protein kinases in apoptosis regulation. Oncogene 2004;23:2838–49.

29. Susin SA, Lorenzo HK, Zamzami N, et al. Molecular characterization of mitochondrial apoptosis-inducing factor. Nature 1999;397:441–6.

30. Joza N, Susin SA, Daugas E, et al. Essential role of the mitochondrial apoptosis-inducing factor in programmed cell death. Nature 2001;410:549–54.

31. Zou H, Li Y, Liu X, Wang X. An APAF-1.cytochrome *c* multimeric complex is a functional apoptosome that activates procaspase-9. J Biol Chem 1999;274:11549–56.

32. Burns TF, El-Deiry WS. The p53 pathway and apoptosis. J Cell Physiol 1999;181:231–9.

33. Degenhardt K, Chen G, Lindsten T, White E. BAX and BAK mediate p53-independent suppression of tumorigenesis. Cancer Cell 2002;2:193–203.

34. Hemann MT, Zilfou JT, Zhao Z, et al. Suppression of tumorigenesis by the p53 target PUMA. Proc Natl Acad Sci U S A 2004;101:9333–8.

35. Symonds H, Krall L, Remington L, et al. p53-dependent apoptosis suppresses tumor growth and progression *in vivo*. Cell 1994;78:703–11.

36. Vogelstein B, Kinzler KW. p53 function and dysfunction. Cell 1992;70:523–6.

37. Rosenzweig T, Ziv-Av A, Xiang C, et al. Related to testes-specific, vespid, and pathogenesis protein-1 (RTVP-1) is overexpressed in gliomas and regulates the growth, survival, and invasion of glioma cells. Cancer Res 2006;66:4139–48.

38. Villunger A, Michalak EM, Coultas L, et al. p53-and drug-induced apoptotic responses mediated by BH3-only proteins puma and noxa. Science 2003;302:1036–8.

39. Johnson TM, Yu ZX, Ferrans VJ, Lowenstein RA, Finkel T. Reactive oxygen species are downstream mediators of p53-dependent apoptosis. Proc Natl Acad Sci U S A 1996;93:11848–52.

40. Uzgare AR, Isaacs JT, Uzgare AR, Xu Y, Isaacs JT. Enhanced redundancy in Akt and mitogen-activated protein kinase-induced survival of malignant versus normal prostate epithelial cells. *In vitro* culturing and characteristics of transit amplifying epithelial cells from human prostate tissue. Cancer Res 2004;64:6190–9.

41. Sanchez AM, Malagarie-Cazenave S, Olea N, et al. Apoptosis induced by capsaicin in prostate PC-3 cells involves ceramide accumulation, neutral sphingomyelinase, and JNK activation. Apoptosis 2007;8:8.

42. Singh SV, Choi S, Zeng Y, Hahm ER, Xiao D. Guggulsterone-induced apoptosis in human prostate cancer cells is caused by reactive oxygen intermediate dependent activation of c-Jun NH2-terminal kinase. Cancer Res 2007;67:7439–49.

43. Watanabe J, Nishiyama H, Matsui Y, et al. Dicoumarol potentiates cisplatin-induced apoptosis mediated by c-Jun N-terminal kinase in p53 wild-type urogenital cancer cell lines. Oncogene 2006;25:2500–8.

44. Maundrell K, Antonsson B, Magnenat E, et al. Bcl-2 undergoes phosphorylation by c-Jun N-terminal kinase/stress-activated protein kinases in the presence of the constitutively active GTP-binding protein Rac1. J Biol Chem 1997;272:25238–42.

45. Yamamoto K, Ichijo H, Korsmeyer SJ. BCL-2 is phosphorylated and inactivated by an ASK1/Jun N-terminal protein kinase pathway normally activated at G(2)/M. Mol Cell Biol 1999;19:8469–78.

46. Thomas A, Giesler T, White E. p53 mediates bcl-2 phosphorylation and apoptosis via activation of the Cdc42/JNK1 pathway. Oncogene 2000;19:5259–69.

47. Lecane PS, Karaman MW, Sirisawad M, et al. Motexafin gadolinium and zinc induce oxidative stress responses and apoptosis in B-cell lymphoma lines. Cancer Res 2005;65:11676–88.

48. Schumacker PT. Reactive oxygen species in cancer cells: live by the sword, die by the sword. Cancer Cell 2006;10:175–6.

49. Trachootham D, Zhou Y, Zhang H, et al. Selective killing of oncogenically transformed cells through a ROS-mediated mechanism by β-phenylethyl isothiocyanate. Cancer Cell 2006;10:241–52.